11th International Symposium on Turbulence and Shear Flow Phenomena (TSFP11)
Southampton, UK, July 30 to August 2, 2019

PRODUCTION OF TURBULENT KINETIC ENERGY IN CURVED SHEAR LAYERS

Daniel M. Moore
Department of Mechanical, Aerospace and Nuclear Engineering
Rensselaer Polytechnic Institute
110 8th Street, Troy NY 12180, USA
moored7@rpi.edu

Michael Amitay
Director, Center for Flow Physics and Control
Department of Mechanical, Aerospace and Nuclear Engineering
Rensselaer Polytechnic Institute
110 8th Street, Troy NY 12180, USA
amitam@rpi.edu

ABSTRACT

An experimental campaign on a bluff body of rectangular cross section, having a side length ratio of 5:1 was carried out using both particle image velocimetry and hot wire anemometry at a Reynolds number of 3.04×10^4. Results show that under a slight angle of attack, the development of unsteadiness in the form of turbulent kinetic energy is significantly altered. Furthermore, the change in shear layer trajectory, due to the angle of attack, mainly affects the initial development of the shear layer instability occurring at the leading edge corner. The consequences of these changes are naturally amplified and result in a difference in shear layer thicknesses of approximately a factor 2 on either side of the body. It is postulated that this imbalance of shear flow entering the wake is circularly responsible for differences found at the leading edge, enforcing the notion of a globally unstable flowfield.

INTRODUCTION

The existence of multiple time and length scales in the wake of bluff bodies has been widely documented by investigators over the past several decades,(Roshko, 1954; Unal & Rockwell, 1988; Prasad & Williamson, 1997). These experimental works justify the observation of select natural phenomena, such as shedding frequencies, with physical governing laws and dimensional analysis forming a phenomenological body of knowledge upon which the community has come to depend. Without these conclusions, the flow around bluff bodies lacks a sense of scale that is essential to understanding the intricacy of these flows.

More scarce are the works that focus directly on the shear layer's natural development of scales. Relative amplitudes of the shear layer momentum thickness to the body dimension indicate that minute changes to the initial conditions of the shear layer leverage relatively larger differences in its behavior as the shear layer enters the wake region. One such change in these initial conditions is the level of free stream turbulence, which itself is represented by a range of scales. Increasing fluctuations in the free stream adds vorticity to the shear layer, manifesting itself through greater entrainment of ambient fluid on the low speed side and reattaching the flow to the side surface more rapidly than in laminar flows, (Bearman & Morel, 1983). However, even under smooth flow conditions, the shear layer over a bluff body contains unifying physical details that link small scales at the leading edge to much larger scales found in the wake. In fact, it appears that the production of Turbulent Kinetic Energy (TKE) necessarily facilitates this migration of scales from small to large. The observed increase in scale magnitude, as shown by the continuous expansion of the shear layer, is initially more rapid than other classical shear layers.

Two important details separate the bluff body shear layer from the 2D planar mixing layer. Growth rates in planar mixing layers exhibit logarithmic or linear trends for laminar or turbulent mixing layers, respectively, (Winant & Browand, 1974). In turbulent scenarios, self-similarity of velocity profiles often assists those attempting to justify the scales that best describe growth, such as momentum or vorticity thickness. Nevertheless, these shear layers are a stronger function of the velocity ratio across it rather than the free stream Reynolds number. To the contrary, the bluff body shear layer has been shown to exhibit higher growth rates (Castro & Haque, 1987), in addition being non-linearly dependent on free stream Reynolds number (Prasad & Williamson, 1997; Lander *et al.*, 2018). The overarching effect of increasing Reynolds number on the bluff body shear layer is to simultaneously shorten the distance to transition, reduce the size of shear layer vortices and increase the shedding frequency. These trends are more easily seen on rectangular prisms than on circular ones, partially due to the streamline distance between separation and the wake. Sharp edges at the leading edge on the square necessitate flow separation independent of the local pressure gradient. For all rectangular bodies, square and otherwise,

the shear layer is born at the leading edge in a direction tangential to the front face which, under zero angle of attack, is perpendicular to the bulk mean flow. This subjects the shear layer to intense levels of curvature, which relaxes with increasing side length ratios, (Shimada & Ishihara, 2001). A common root of these two trends, elevated growth rates and Reynolds number dependence, is the development of TKE. The work presented in this paper focuses on the natural development of TKE for a shear layer over a 2D prism having side length ratios $L/h = 5$ at a fixed Reynolds number, $Re_h = 3.04 \times 10^4$. The following sections aim to move toward a universal description of the flow by providing a physical link between activity at or near the front face of the body, and activity in the wake.

EXPERIMENTS

A rectangular prism was fabricated at Rensselaer Polytechnic Institute (RPI). The model was machined from aluminum, with final dimensions of $L = 254\,\text{mm}$, $h = 50.8\,\text{mm}$ and a span of $w = 508\,\text{mm}$. The model was mounted on a circular shaft between end-plates that allowed the model to change its inclination angle relative to the oncoming wind. End-plates extended approximately $14h$ upstream and $20h$ downstream of the model's rotational axis. The test rig, including the model along with end-plates, was installed in the Large Subsonic Wind Tunnel at the Center for Flow Physics and Control (CeFPaC) at RPI.

The wind tunnel itself is a blow-down type with two centrifugal fans powered by a 100 hp motor. A large settling chamber houses a honeycomb and a series of screens with decreasing grid size, which act to break up larger turbulent eddies and distribute the flow uniformly before the flow is accelerated through the contraction into the test section. The contraction has an area reduction ratio of 9 : 1 with the test section having dimensions of height, width, and length of 0.8 m, 0.8 m, and 5.0 m, respectively. In the empty tunnel, the uniformity of the mean flow across the middle 0.5 m of the tunnel is better than 0.1%, with lower velocities in regions close to the walls. Over the range of wind speeds used for testing, the longitudinal turbulence intensity was measured to be less than 0.25%. Tests were carried out at a range of Reynolds numbers varying between 1.34×10^4 to 1.18×10^5 by changing the speeds, U_∞ although only one Reynolds number is reported here for brevity. The Reynolds number in this case is based on the dimension of the model height, the freestream velocity and the kinematic viscosity of the air in the tunnel, $Re_h = U_\infty h/\nu$. The blockage ratio under orthogonal configurations was 6.2%.

In order to support a high level of spatial resolution using Particle Image Velocimetery (*PIV*), multiple Fields of View (*FOVs*) were acquired. One *FOV* encompassed the entire body length using a 35 mm lens. The other used a 200 mm lens and zoomed into the region near the leading ledge. Each *FOV* was investigated using two-component *PIV*. The camera was a LaVision Imager LX camera, with 2 MPx resolution. The flow was illuminated with a New Wave Solo *PIV* 120mJ/pulse per frame Nd-YAG ($532\mu m$) dual-head laser. The timing of the system allowed sampling at approximately 15 Hz and in all cases the convergence of turbulent statistics was satisfied by acquiring 1000 image pairs. Vector fields were calculated using sequential cross-correlations of the image pairs. For both camera setups, a multipass processing algorithm was implemented through LaVision software. For the smaller *FOV* the first pass used a $64 \times 64\,\text{px}$ interrogation window, while the secondary and final passes used a $32 \times 32\,\text{px}$, each with a 50% overlap. The resulting vector fields had a spatial resolution of 5.45 vectors per millimeter. This meant that each *FOV* corresponded to a physical domain of $0.35h \times 0.88h$ or a total of 279.4 vectors per body height. The larger *FOV* used a $48 \times 48\,\text{px}$ interrogation window with a 50% overlap, while the secondary and final passes used a $24 \times 24\,\text{px}$, with a 75% overlap. The resulting vector fields there had a spatial resolution of 0.9 vectors per millimeter.

Additional point measurements in the flow were carried out using a Dantec 55P11 single hot wire probe. The wire was individually calibrated over a wider range of velocities than those analyzed here and mounted on its own traverse system located beneath the wind tunnel along the centerline of the model. The traverses had a repeatability of 5 μm in both streamwise and vertical coordinates. The probe was sampled at 40 kHz for 60 seconds and stationed at locations along the time-averaged shear layer, as determined from the results of the processed *PIV* data. The procedure to locate the hot wire involved identifying the origin (at the leading edge corner) and using the topology of the reconstructed *PIV* field to get a series of target locations in the coordinates of the *PIV*.

RESULTS

Figure 1 shows the time-averaged streamlines, obtained from PIV measurements, over the model at $\alpha = 0^\circ$ and 5°. For both cases, the streamlines show the large areas of recirculating flow alongside the body. In figure 1a the dividing streamline on the lateral sides of the body is colinear with the time-averaged shear layer position, a point that will be addressed in subsequent paragraphs. In figure 1a, at $\alpha = 0^\circ$ where the data on upper and lower halves are mirrored, the recirculation area extends over most of the body terminating at $x^* = 4.4$ (* notation is used for non-dimensional parameters that use the body height h and/or freestream velocity U_∞). When the angle of attack is increased to $\alpha = 5^\circ$ as in figure 1b, the flow field over the model is vastly different on either side. On the pressure side, the reattachment length is reduced approximately by a factor 2, whereas on the suction side, the flow is completely separated and does not reattach, resembling the flow of bluffer bodies whose L/h ratio is less than approximately 3. In each of these scenarios the shear layer is curved, with a radius of curvature that continuously relaxes with downstream distance and the streamlines fall into alignment with the mean flow.

Under these flow conditions, the flow transitions to turbulence within the shear layer. The work recently published by Lander *et al.* (2018) has shown that the observed frequency of instability waves are of a Kelvin-Helmholtz type mechanism. The frequency behavior with respect to a changing Reynolds number is balanced by the corresponding momentum thickness and velocity ratio across the shear layer at the transition point. The shear layer position and transition point itself are defined using the maxima of TKE in the flowfield. The same definitions are employed here using a two dimensional representation, $\tilde{E} = 1/2(\overline{u'u'} + \overline{v'v'})$, although neither the locus of position nor its maximal values are plotted. Instead, figure 2 is presented, where the integrated $\tilde{E}$ values highlight the difference in accumulation of TKE along the shear layer. In all cases, the rise of $\tilde{E}$ is exponential and steep initially, swiftly covering an order

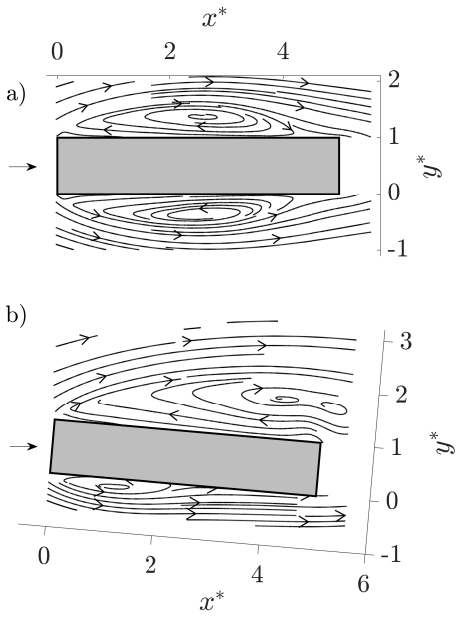

Figure 1. Time-averaged streamlines over a 5:1 body at $Re_h = 3.04 \times 10^4$. (a) $\alpha = 0°$, and (b) $\alpha = 5°$.

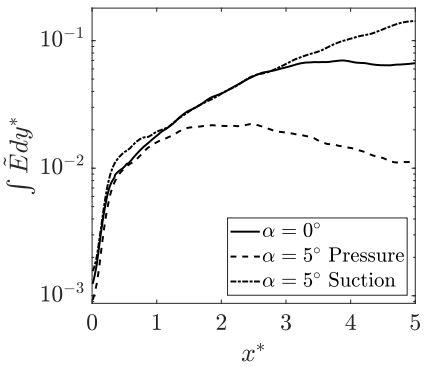

Figure 2. Integrated turbulent kinetic energy along the 5:1 body. $Re_h = 3.04 \times 10^4$.

of magnitude, followed by a subsequent reduction in slope at approximately $x^* \approx 0.5$ for various distances among the three cases. The initial rise in TKE is due to the amplification of the shear layer's Kelvin Helmholtz (KH) instability. The slope reduction location coincides with the turbulent transition length for these shear layers. Beyond this point, further accumulation of TKE is due to the magnitude of the production term in the TKE transport equation, sustained by substantial shear near the boundary of the recirculation region along with increasing fluctuation amplitudes. Locations of negative slope, $\partial/\partial x^*$, match with the reattachment locations of the mean flow as shown earlier, where the shear layer on the pressure side of the $\alpha = 5°$ and both alongside $\alpha = 0°$ are relevant. That the initial reduction in slope is concurrent with the saturation of the shear layer instability, a detail which is explored below.

In order to describe the shear layer behavior in an efficient and effective manner its position and content must be characterised. The following transformation performed

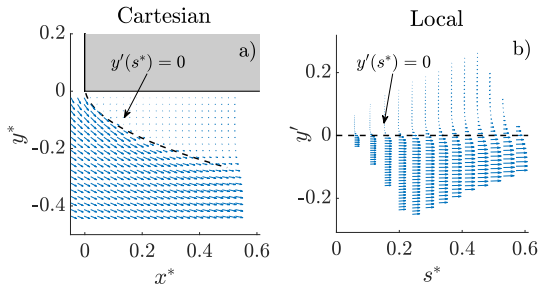

Figure 3. Velocity vectors in the vicinity of the leading edge, represented by (a) Cartesian coordinates, and (b) Local coordinates. Time-averaged shear layer position is described by the dashed line $y'(s) = 0$. $Re_h = 3.04 \times 10^4$.

in figure 3 is used as one way to simplify the number of parameters needed to describe the shear severity within the shear layer. Figure 3a shows the traditional vector field for the time-averaged flow near the leading edge corner. The degree of shear is described here with both components of velocity, $U = U(x^*, y^*)$, along a trajectory specified by both x^* and y^*. To simplify this scenario and geometrically unwrap the shear layer in the regions nearest the leading edge, a local coordinate system is used (figure 3b). The shear layer position, in both scenarios, is indicated by the dashed line. In the Cartesian reference frame, the shear layer is curved. A local coordinate can be specified at each streamwise location with a tangent vector, s^*, and a normal vector, y', each at an angle with respect to the original axes. On interpolating the original fields onto the new local axes and rotating the velocity vectors by the corresponding angles, the local coordinate system is completed and the shear layer is represented along the line $y' = 0$. This transformation also eases the calculation of the shear layer quantities like momentum thickness, θ^* and velocity ratio $\mathcal{R}$, by representing shear severity with a single component of velocity, $U = U(y')$. The transformation needs only be applied in the regions nearest the leading edge. Everywhere else, the radius of streamline curvature exceeds 5 or even 10 body dimensions such that a Cartesian description remains satisfactory.

Extracting information about the growth of specific frequencies in the flow, was done with a hot wire probe positioned along the shear layer trajectories, highlighted in figure 3. For each case along these trajectories, samples were taken such that the power spectrum could be calculated and monitored as it evolved along the local coordinate. It is noteworthy that the resulting spatial resolution is 140 measurements per body dimension. The series of spectra was then divided into bins of 50 Hz and averaged such that each bin represented a frequency band whose power could be plotted a function of distance along the shear layer. This procedure most simply allows the spatial amplification rates of each frequency to be easily observed, thereby identifying themselves as unstable ones. Singularly, the frequency bin with the steepest slope is defined by f_{KH}.

The combination of a local transformation and resulting hot wire measurements allows for the direct comparison of these curved shear layers with the more classical ones, such as the planar mixing layer. In order to make this comparison, several subordinate parameters are needed. These parameters are plotted in figure 4. Near the lead-

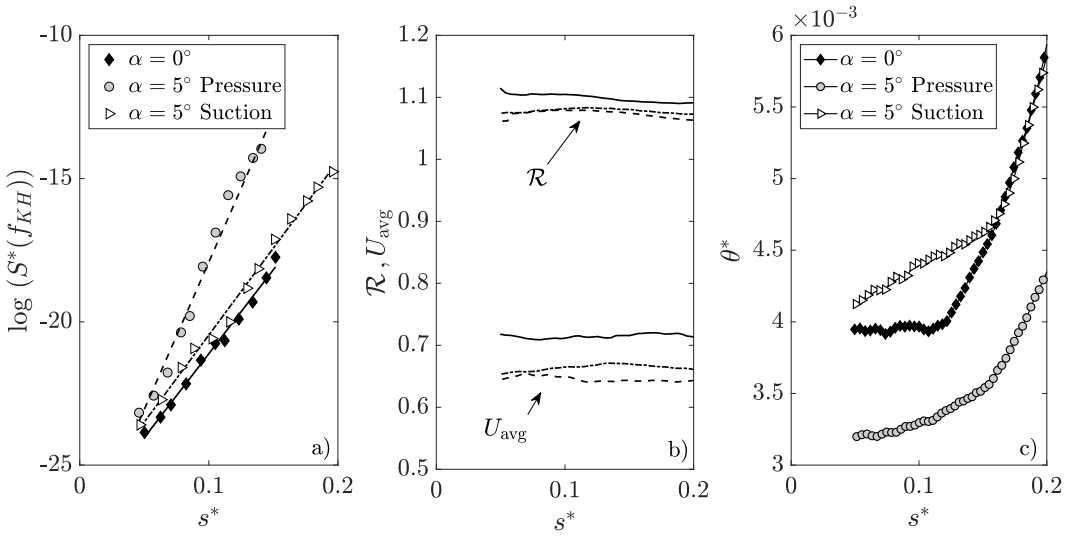

Figure 4. Constants used to non-dimensionalise growth rates. (a) Power Spectra values, $S^*(f_{KH})$, (b) velocity ratio, $\mathcal{R}$ and average velocity U_{avg}, and (c) momentum thickness, θ^*.

ing edge corner, the amplification rate of the most unstable frequency may be described by an exponential curve, synonymous with the linear growth of small disturbances. Using a logarithmic representation along the local coordinate s, figure 4a shows the growth rates of f_{KH} for the three shear layers analysed here. For each data set, a fitting curve shows the robustness of the assumption about linear disturbances. In general, the fit is good. Incorporating data points farther downstream results in increasing deviations from the fit curves. Points upstream of those plotted here are nearly constant values, resting just above the noise floor of the hot wire measurement system. The resulting data set that is shown here is a best estimate for the range where the growth of this disturbance is assumed to be a linear mechanism. Over that same range, figure 4b shows the velocity ratio gained from the local PIV fields defined by $\mathcal{R} = (U_{\max} - U_{\min})/U_{\text{avg}}$ as well as U_{avg} itself, which is defined as, $U_{\text{avg}} = 0.5\,(U_{\max} + U_{\min})$. The velocities $U_{\max}, U_{\min}$ are found on the high and low speed sides of the shear layer, respectively. Upon inspecting the velocity ratios, it becomes immediately clear that $\mathcal{R} > 1$ everywhere. This is indicative of recirculating flow, something that planar mixing layers do not experience and therefore $\mathcal{R}$ never exceeds unity in those cases. Lastly, the values of the momentum thickness are presented in figure 4c for the three shear layers. Planar mixing layers abide by the behavior identified in Winant & Browand (1974) where the growth appears linear when the layer is turbulent. The data in the current study show that all three shear layers exhibit exponential growth of momentum thickness initially. In the immediate regions near the leading edge as shown in figure 4c the corresponding increase is relatively small over the first $0.15h$. Beyond that point, the exponential growth accelerates the size the momentum thickness significantly. This has been seen before for the 1:1 square by Lander *et al.* (2018) who explained that the growth is not only exponential in space, but non-linearly depends on Reynolds number, a feature that is typically associated with wall-bounded flows rather than free shear layers. In the current study, the surface of the model, or *the wall*, is only a handful of momentum thicknesses away from the place of calculation leaving the door open for those who wish to study the nearby influence of boundaries on nominally free shear layers.

Nevertheless, the magnitude of the momentum thicknesses presented reflect the importance of the small scales at the leading edge, namely those less than 1 percent of the body dimension. None of the data in figure 4 begin exactly at the origin as the linear fitting procedure only fits well beyond $s^* > 0.05$, suggesting either that there is a critical distance to transition, or the levels of fluctuations are beneath the resolution of the anemometer. However, they do show that each shear layer scenario contains values that are nearly constant or weakly increasing over the first 15% of the body height. The amplification rate in this domain, velocity ratios and corresponding momentum thicknesses are well represented by average values. As such, average values of each of these curves are extracted to non-dimensionalise the growth rates over the same physical domain.

The resulting distribution of all spatial growth rates are plotted in figure 5 for the shear layers on a 5:1 body, for $\alpha = 0°$ and $5°$. In addition to the experimental data for these bluff body shear layers, the solution to the hydrodynamic instability of the hyperbolic tangent profile is included from the spatial analysis in Michalke (1965). The hyperbolic tangent velocity profile is widely accepted as one continuous form of the self-similar velocity profiles for planar mixing layers, and can be used in solving the Rayleigh equation for small disturbances. With that in mind, it is employed here as an analytical solution to a flow that is well predicted by linear theory. For the experimental data, the fitting curves previously discussed are used to generate the data points in figure 5. Recognizing that instability waves may be described in a spatial sense using normal modes, $\phi \propto e^{i(kx-\omega t)}$ where k is a complex wave number and ω is a real frequency, the increasing slopes in figure 4a may be used as an analog for the imaginary component, $-k_i$. Slopes are rendered dimensionless by the initial values of the momentum thickness and velocity ratio. Frequencies have a similar dimensional reduction, using the the average velocity. As stated, the velocity ratio is more than one in all shear layers tested here, in effect attenuating these curve amplitudes. On the other hand, the velocity ratio for Michalke's solution is exactly 1.

In general, the curves show familiar distribution patterns where the band of frequencies that appear to grow unstably support a global maximum, which was identified earlier by f_{KH}. Specifically, the baseline case of $\alpha = 0^\circ$ shares a similar frequency band with the planar mixing layer (e.g. frequencies beyond $f\theta/U_{\text{avg}} > 0.1$ do not appear to grow). However, on inspecting the amplitudes, the bluff body shear layer shows more aggressive growth than the mixing layer. Without the reduction by $\mathcal{R}$ the difference in amplitudes would further increase by more than 10%. It was reminded in Monkewitz & Nguyen (1987) that curvature in bluff body shear layers, where the high speed side is on the outside of the curve, ought to have a suppressing effect, reducing the growth of the instability. This is in contrast to flows where the high speed side may reside on the inside of the curve in which case the growth rates are elevated. Here, it appears that if the curvature of the bluff body shear layer is reducing growth rates, there must be another mechanism opposing this reduction even more so.

This suspicion is reinforced by comparing the baseline, $\alpha = 0^\circ$, case to the case of $\alpha = 5^\circ$. Streamlines initially shown in figure 1b demonstrate that the curvature of streamlines on the pressure side of the body are more severe than those on the suction side. However, the growth rates indicate that the pressure side boasts the highest growth rates, nearly three times more than the planar mixing layer solution. So too is the frequency range extended compared to the planar mixing layer, with higher frequencies becoming more competitive by exhibiting elevated amplification rates in the cases of the non-zero angle of attack. It is interesting to see that the value extracted as f_{KH} on the suction is twice that of the pressure side at $f\theta/U_{\text{avg}} = 0.026$, and 0.049, respectively. The appearance of two local maxima for the pressure side distribution is a detail that was initially unexpected. Additionally, the peaks are curiously close to multiples of one another at 0.026 and 0.078. Arrows in the figure indicate integer multiples of the peak frequency on the pressure side distribution. Appealing to the literature, Lyn & Rodi (1994) have considered the validity of the sub-harmonic growth model via collective interaction in the presence of wake shedding behind a square prism. Their analysis found the wake shedding to be an unlikely candidate for the excitation of sub-harmonics within the shear layer, a result that is considered relevant to the current scenario. Moreover, the current set of results is reserved for the physical space upstream of the first observed vortex through instantaneous PIV images (not shown). As such, the existence of these multiple concentrated bands of spatial amplification remain an open area of interest to the authors. From a phenomenological perspective, the higher frequency content may be partially explained by the thinner momentum thickness near the leading edge, a parameter that appears to be integral to the flow both at large and small scales.

Earlier figures have indicated that the length scale relevant to transition is that of the momentum thickness of the shear layer. This is well below the length scale needed to describe the wake, typically the body dimension via a wake Strouhal number. Thus, there exists a magnitude gap of nearly three orders between the dominant length scale at the leading and trailing edges. Furthermore, it is logical to expect that the angle of attack exerts considerable influence on the development of the shear layer in the space between these two areas, similar to the TKE. Figure 6 attempts to answer this by comparing momentum thickness over the entire side length of the 5:1 body. Proper depiction of the true

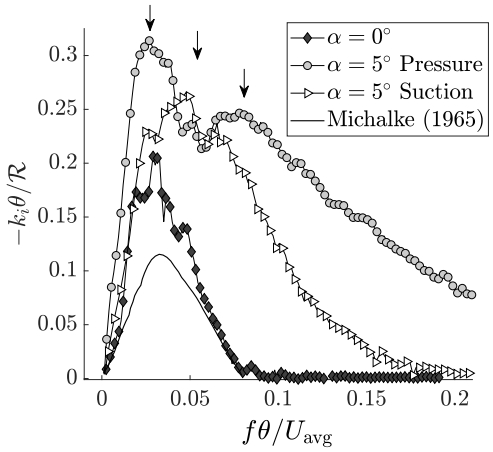

Figure 5. Growth rates of the shear layer instability for the 5:1 body. Solid line is the theoretical solution to the hyperbolic tangent velocity profile. Every other point is plotted.

gradients across the shear layer requires a piece-wise effort. Close to the leading edge, $x^* < 0.4$, the local coordinate system is used to calculate values of θ^* and then projected back onto a Cartesian x^* axis for comparison. Beyond $x^* \geq 0.4$ the calculation is performed in the Cartesian frame. Had the latter method been applied universally, values near the leading edge would appear artificially inflated. In general, the agreement and limited overlap of these two data sets is approximately within 2% of the largest values. This is verified using the zoomed-in inset within the figure showing the boundary between local and Cartesian calculations.

The combined effect in figure 6 resembles similar overall trends of the TKE presented in figure 2 where the body at an angle of attack of 5° has significantly faster or slower development rates for the suction or pressure side of the body, respectively. The suction side, which is the only shear layer among the three analysed to remain completely separated along its entire length, shows growth of momentum thickness that could be reasonably approximated by a linear fitting procedure. The other two, having increasing streamline curvature for the baseline case and the pressure side, show diminishing increases. These global behavior are contrary to what was found in the region close to the leading edge where the slopes of these curves fit a power law with exponents higher than 1. It follows that there must be an acute reduction in slope between these two growths. However, the associated physics behind that location are not dwelt upon here. Instead, focus is given to the connection made between leading edge and wake region. From figure 6 it begins to become clear that the shear layer transition process takes place at scales less than 1 percent of the body dimension, a process that eventually takes on a pivotal role in the global development of the shear layer as it matures to sizes similar to those of the body.

DISCUSSION

Simultaneously studying the global behavior of the shear layer as well as the small regions immediately adjacent to the leading edge corner allows for the tracking of length scale migrations, which so far have largely eluded bluff body descriptions. Crucial to these flows, and to the descriptions they share, is the behavior of the shear layer.

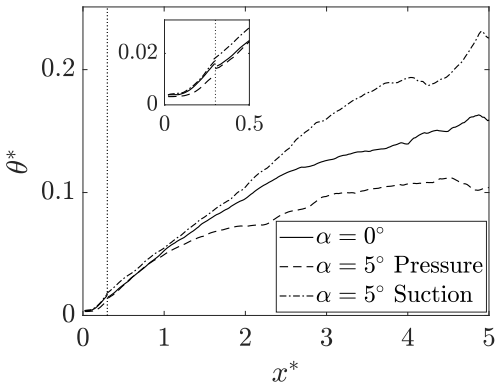

Figure 6. Downstream evolution of the momentum thickness of the shear layer on a 5:1 body. The vertical dashed line indicates the boundary for where Cartesian and Local coordinate systems meet.

In support of this narrative, this paper submits the following findings and conclusions. The shear layer, under low turbulence free stream conditions at a constant Reynolds number, exhibits unique behavior that prevents it from being fully represented by planar mixing layer knowledge. Specific to the bluff body shear layer is a steep pressure gradient at separation, a continuously changing amount of flow curvature, recirculation on the low speed side, and potential for coupling with downstream global instabilities. To account for these effects, corrections are implemented with limited success at matching experiments with the analytical solution. Local coordinates geometrically unwrap the shear layer to account for curvature. Normalizing growth rates by $\mathcal{R}$ correct for the effects of recirculation. And the possibility of a coupled disturbance is reduced by testing an extended body, ($L/h = 5$ as opposed to a bluffer body $L/H \approx 1$) in an attempt to isolate the shear layer from the wake. Admittedly, the pressure gradient and associated vorticity flux remain unaccounted for at this point. This series of corrections, fails to collapse the data, suggesting that the shear layer is in need of a revised phenomenological description.

Recent studies by this same group have published on the scaling of the transitioning shear layer over a 2D square prism ($L/h = 1$) and further pointed out that in the regions near the leading edge corner, the shear layer and the front face boundary layer exhibit similar behavior under a changing Reynolds number suggesting a level of communication between the two, (Lander *et al.*, 2018). This is in an important finding because it points towards the continuous nature of the flow field, even over a discontinuous edge. If the bluff body shear layer cannot be explained using a planar mixing layer analysis alone, perhaps further knowledge of the front face boundary layer will shed new light on the true nature of the flow. Specifically, the vorticity dynamics around corner are of great interest.

At present, the manifestation of vorticity is seen by changing the angle of attack of the body. Changing the angle of attack has two primary effects on the shear layer. First, the wake vortices are skewed in their position and strength due to a difference in shear layer development. On the suction side, the flow is completely separated beginning at the leading edge. The shear layer freely expands and diffuses vorticity before entering the wake. On the pressure side, the flow reattaches to the lateral face, altering the vorticity budget before re-separating at the trailing edge. Second, the front face boundary layers must also react to this change in angle. Pressure gradients at separation are reduced at the corner of the suction side and increased at the pressure side. This happens at the same time that the stagnation point shifts to compensate for the angle of attack. These two effects combine to generate different amounts of vorticity, perhaps driving the difference in growth rates explored earlier. This complicated flowfield quickly forms a positive feedback loop. Changes in each shear layer's transition modulate the width of the layer by the time it passes the trailing edge, supporting an asymmetric wake. That asymmetry is communicated to the front face, which further changes the vorticity concentration in the separated shear layer, facilitating different growth rates on the pressure/suction sides. This continuous pattern also links small scales (high frequencies) at the leading edge with the larger ones in the wake, underscoring a shear layer instability that is inherently coupled by some finite amount to other instabilities in the flowfield.

REFERENCES

Bearman, P. W. & Morel, T. 1983 Effect of free stream turbulence on the flow around bluff bodies. *Progress in Aerospace Sciences* **20** (2-3), 97–123.

Castro, I.P. & Haque, A 1987 The structure of a turbulent shear layer bounding a separation region. *Jounral of Fluid Mechanics* **179**, 439–468.

Lander, D.C., Moore, D.M, Letchford, C.W. & Amitay, M. 2018 Scaling of Square Prism Shear Layers. *Journal of Fluid Mechanics* **849**, 1096–1119.

Lyn, D & Rodi, W 1994 The flaping shear layer formed by flow separation from the forward corner of a square cylinder. *Journal of Fluid Mechanics* **267**, 353–376.

Michalke, A. 1965 On spatially growing disturbance in an inviscid shear layer. *Journal of Fluid Mechanics* **23**, 521–544.

Monkewitz, P. A. & Nguyen, L. N. 1987 Absolute instability in the near-wake of two-dimensional bluff bodies. *Journal of Fluids and Structures* **1** (2), 165–184.

Prasad, A. & Williamson, C H K 1997 The instability of the shear layer separating from a bluff body. *Journal of Fluid Mechanics* **333**, 375–402.

Roshko, A 1954 On the drag and shedding frequency of two-dimensional bluff bodies. *Tech. Rep.*. National Advisory Committee for Aeronautics, Washington.

Shimada, K. & Ishihara, T. 2001 Application of a modified k-e model to the prediction of aerodynamic characteristics of rectangular cross-section cylinders. *Journal of Fluids and Structures* **16** (15), 399–413.

Unal, M F & Rockwell, D 1988 On vortex formation from a cylinder. Part 1. The initial instability. *Journal of Fluid Mechanics* **190**, 491–512.

Winant, C. D. & Browand, F. K. 1974 Vortex pairing : the mechanism of turbulent mixing-layer growth at moderate Reynolds number. *Journal of Fluid Mechanics* **63** (02), 237–255.